OPEN ACCESS

University of BRISTOL

Luterbacher Mus, R., Trask, R., & Bond, I. (2015). Static and fatigue tensile properties of cross-ply laminates containing vascules for self-healing applications. *Smart Materials and Structures*, *25*(1), [015003]. https://doi.org/10.1088/0964-1726/25/1/015003

Publisher's PDF, also known as Version of record

License (if available):
CC BY

Link to published version (if available):
10.1088/0964-1726/25/1/015003

Link to publication record in Explore Bristol Research
PDF-document

This is the final published version of the article (version of record). It first appeared online via IOP Publishing at http://dx.doi.org/10.1088/0964-1726/25/1/015003. Please refer to any applicable terms of use of the publisher.

University of Bristol - Explore Bristol Research
General rights

This document is made available in accordance with publisher policies. Please cite only the published version using the reference above. Full terms of use are available:
http://www.bristol.ac.uk/red/research-policy/pure/user-guides/ebr-terms/

IOPscience iopscience.iop.org

Home Search Collections Journals About Contact us My IOPscience

Static and fatigue tensile properties of cross-ply laminates containing vascules for self-healing applications

This content has been downloaded from IOPscience. Please scroll down to see the full text.

2016 Smart Mater. Struct. 25 015003

(http://iopscience.iop.org/0964-1726/25/1/015003)

View the table of contents for this issue, or go to the journal homepage for more

Download details:

IP Address: 137.222.138.5
This content was downloaded on 22/07/2016 at 15:42

Please note that terms and conditions apply.

OPEN ACCESS
IOP Publishing
Smart Materials and Structures
Smart Mater. Struct. **25** (2016) 015003 (10pp)
doi:10.1088/0964-1726/25/1/015003

Static and fatigue tensile properties of cross-ply laminates containing vascules for self-healing applications

R Luterbacher, R S Trask and I P Bond

Advanced Composites Centre for Innovation and Science, University of Bristol, Queen's Building, Bristol BS8 1TR, UK

E-mail: rafael.luterbachermus@bristol.ac.uk

Received 1 July 2015, revised 24 September 2015
Accepted for publication 19 October 2015
Published 17 November 2015

Abstract

The effect of including hollow channels (vascules) within cross-ply laminates on static tensile properties and fatigue performance is investigated. No change in mechanical properties or damage formation is observed when a single vascule is included in the 0/90 interface, representing 0.5% of the cross sectional area within the specimen. During tensile loading, matrix cracks develop in the 90° layers leading to a reduction of stiffness and strength (defined as the loss of linearity) and a healing agent is injected through the vascules in order to heal them and mitigate the caused degradation. Two different healing agents, a commercial low viscosity epoxy resin (RT151, Resintech) and a toughened epoxy blend (bespoke, in-house formulation) have been used to successfully recover stiffness under static loading conditions. The RT151 system recovered 75% of the initial failure strength, whereas the toughened epoxy blend achieved a recovery of 67%. Under fatigue conditions, post healing, a rapid decay of stiffness was observed as the healed damage re-opened within the first 2500 cycles. This was caused by the high fatigue loading intensity, which was near the static failure strength of the healing resin. However, the potential for ameliorating (via self-healing or autonomous repair) more diffuse transverse matrix damage via a vascular network has been shown.

Keywords: self-healing, fibre reinforced polymer, cross-ply laminate, matrix damage

(Some figures may appear in colour only in the online journal)

1. Introduction

The topic of self-healing materials has been an area of increasing interest for researchers in the materials science sector over the past 15 yr. Several extensive reviews [1–4] exist in the literature. With regards to the application of self-healing in fibre reinforced polymer (FRP) composites, Norris *et al* [5] highlighted the potential for reducing conservative safety margins following impact damage in FRPs. In essence, two different self-healing approaches exist: (1) intrinsic and (2) extrinsic. The former relies on the ability of the matrix material to restore its mechanical properties by a reversible reaction or via a remendable polymer [6]. Yang *et al* [7] showed that carbon-epoxy aerospace-based T-joints can be both toughened and repaired using such mendable thermoplastic stitches. The benefit of this healing approach is highlighted by the ability to realize multiple healing events, however, the main drawback is the adulteration of the matrix system or the introduction of a new material phase, which could lead to increased processing/certification costs. In addition, an external stimulus is typically needed to activate the healing reaction, e.g. heat. The second extrinsic approach concerns the introduction of new 'repair' materials, generally in liquid form, either through embedded microcapsules [8] or through internal capillaries in the structure. The first generation of capillaries were hollow glass fibres [9–11] that entrained the healing agent, in a similar way to

Content from this work may be used under the terms of the Creative Commons Attribution 3.0 licence. Any further distribution of this work must maintain attribution to the author(s) and the title of the work, journal citation and DOI.

 © 2016 IOP Publishing Ltd Printed in the UK

microcapsules. These embedded fibres had the advantage of being easier to embed within a FRP composite and offered more scope for incorporating a greater volume of healing agent. These two healing approaches have the benefit over an intrinsic approach in that a 'reactive' healing agent is released upon a damage event occurring. This action results in an interaction with the propagating damage, thereby, reducing the need for an external stimulus. However, the inherent drawbacks are (1) the limited healing agent volume and (2) that the healing agent must be incorporated during manufacture. This means that it has to survive the manufacturing/processing conditions of the host material and that the shelf life of the healing agent has to be superior to the design service life of the host material [12, 13]. An additional shortcoming is that active chemistries are typically employed as healing agents meaning that multi-components must be kept separate until required, and often stoichiometric rules must be met [14].

The current generation of capillaries utilizes a hollow channel network [15]—hereafter referred to as vascules. These have the benefit of introducing the healing agent only upon a damage event, meaning that bigger volumes can be infused and that the healing agent does not have to survive the host material processing. In addition, the vascular network can be used for other multifunctional applications such as thermal management [16] and/or structural health monitoring (SHM) [17].

Vascular networks are manufactured by the introduction of a preform which is removed after curing [18–20]. One dimensional, two dimensional and three dimensional networks have been reported [21, 22].

By placing the preform into cut-outs within prepreg plies, the size of any resulting resin pockets adjacent to these disruptive additions is reduced [18]. These features limit the potential for resin pockets to act as damage initiators [23], whilst also ensuring the introduction of the vascular network does not bias the mechanical performance of the host structure. Vascules placed perpendicular to the propagation direction of delaminations have been shown to increase the fracture toughness both in mode I and mode II. However, a knockdown in strength was observed when vascules were oriented normal to load bearing plies [24]. Conversely, when vascules are located in the propagation direction, no influence was observed [19]. For small vascule diameters (below 0.5 mm), the vascules do not show any detrimental effect on the compressive strength when placed into pre-formed cut-outs in unidirectional laminates [18]. Similar results were found by Kousarkis *et al* [25, 26] who studied the effect of vascule size on interlaminar shear, impact, tensile and compressive loading. The damage mechanism due to longitudinal compressive loading was studied by Huang *et al* [27]. During these studies the preforms were not placed in a cut-out region thereby introducing detrimental fibre waviness and wrinkling, amplifying the detrimental effect of the incorporated vasculature. Coppola *et al* [28] reported that a 3D vascular network in a 3D woven glass/epoxy composite has a negligible impact on static tensile properties. The studies herein have focused on placing the vascules in plies oriented in the same direction.

As reported extensively in the open literature [29–32], the failure mechanisms of FRP composites are highly complex due to their hierarchical nature, encompassing fibre-matrix debonding, matrix damage (both intralaminar and interlaminar) and fibre failure. Whereas repair of the latter is out of the scope of what can currently be achieved for the aforementioned self-healing systems, addressing the different matrix failure types [33] could postpone final failure of the component, and thereby increase the service life. Delaminations (interlaminar matrix damage) are considered to be a critical damage mode in FRPs and a variety of self-healing studies have addressed this damage mode [12, 19, 34, 35]. However, limited studies exist which address fibre debonding [36] or intralaminar damage [37, 38].

The latter is responsible for delamination migration in multi-angle laminates [39] and also acts as a delamination initiator or promotes fibre failure at ply interfaces [40]. Transverse damage has been extensively studied as a damage mechanism in cross-ply laminates [30, 31, 40, 41] and this laminate configuration seems suitable for investigating how this damage type can be addressed with a self-healing approach [37, 38]. Within cross-ply laminates the first damage mechanism is transverse matrix failure [41], followed by delamination initiation and propagation at the 0/90 interface. These damage mechanisms lead to stress concentrations and fibre breakage [40]. In some cases, instead of delamination initiation, oblique transverse cracks are observed [31].

Thus, the aim of this research is twofold:

- Firstly, to investigate the effect of vascules on the innate mechanical performance of FRPs, both in tensile static and fatigue loading, and to explore the influence on damage formation. In order to introduce the vascules, the ply structure is disturbed and could potentially lead to the formation of a different damage morphology within the sample. Assessing, the impact of the vascule on the mechanical performance and damage formation is important as the introduction of the additional functionality should not be detrimental to the global behaviour.
- Secondly, to investigate the potential for mitigating the effect of transverse matrix damage on the mechanical properties both under static and fatigue loading by a process of extrinsic self-healing. This comprises the injection of a low viscosity healing agent into the vascule in order to infuse and ameliorate the transverse damage.

2. Materials and experimental details

2.1. Laminate manufacture

Specimen geometry and vascule positioning within the laminate are shown in figure 1. For ease of damage visibility via backlight illumination, specimens were manufactured using E-glass/epoxy (E-glass/913, Hexcel UK) prepreg by hand lay-up. It is worth noting that the fibre type does not play a critical part in this study, and findings are expected to be generally applicable. The selected lay-up was $[0_4/90_4]_S$. The panels were fabricated following the manufacturer's recommended curing cycle (60 min at 125 °C and 700 kPa with a ramp rate of 2 °C min^{-1}).

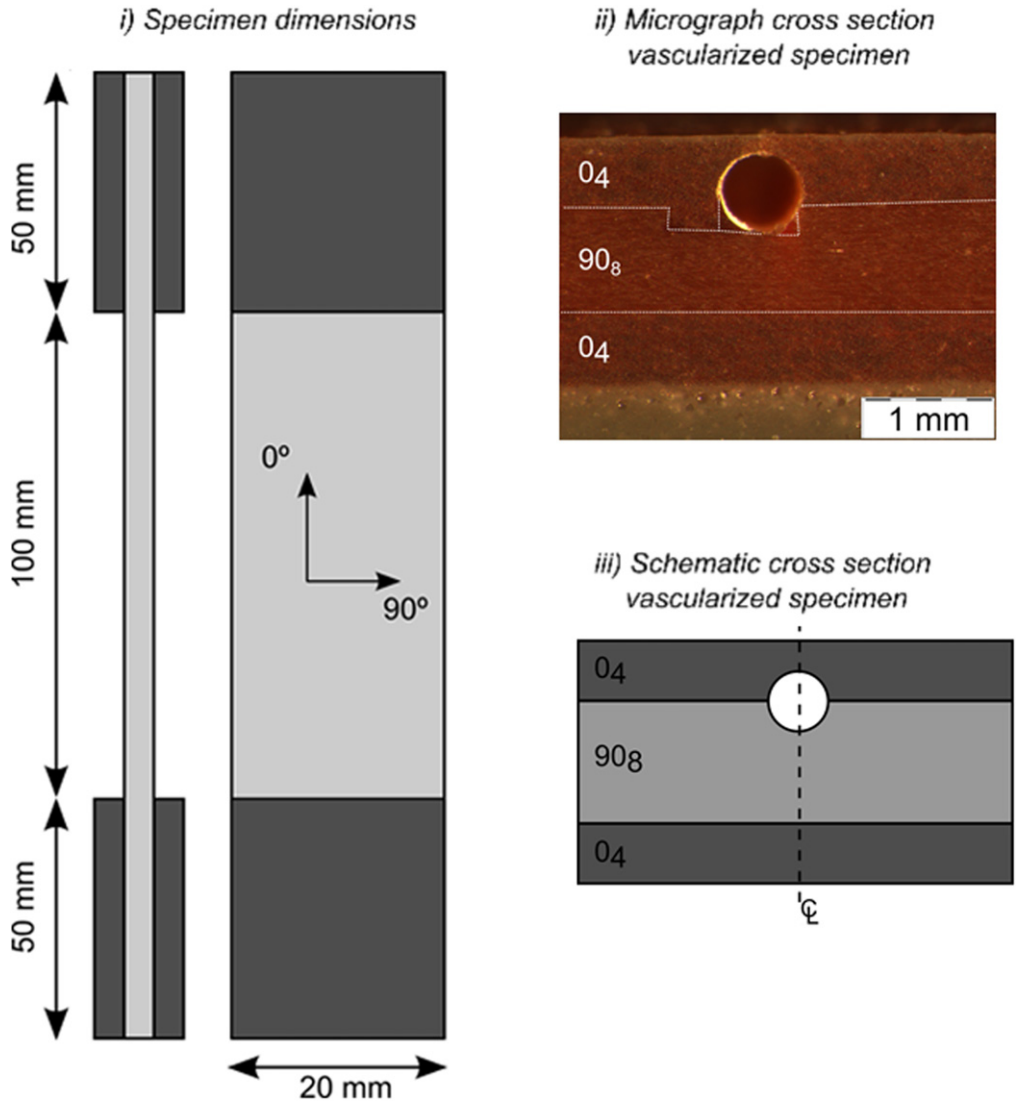

Figure 1. Specimen details: (i) specimen dimensions, (ii) micrograph and (iii) schematic of the cross section of a vascularized specimen.

The plies containing vascules ($0_2/90_2$) had a section removed and PTFE coated nickel chromium wires (diameter 0.56 mm) were placed between these cut-outs according to the manufacturing method 'B' proposed by Norris *et al* [18]. Once the laminate was fully cured, the wires were removed and 50 mm long glass fibre end tabs were secondary bonded to the laminate (top and bottom; front and back), before individual specimens were then machined to size (figure 1).

2.2. Mechanical testing

A Schenck Hydropuls® PSA universal testing machine, equipped with a calibrated load cell of 75 kN was used for all testing. Backlight illumination was used for damage monitoring whilst an Olympus SZX 16 microscope with a ColourView camera was used for optical microscopy. Edge damage pattern was inspected using a scanning electron microscope (SEM: Hitachi TM3030 table top microscope).

2.2.1. Static testing. Static tests to failure were performed according to ASTM D3039 [42] at a test rate of 2 mm min^{-1}. Strain was recorded using a video extensometer (Imetrum) on the central 50 mm region of the specimen for the stress range of 20–100 MPa. This stress range was selected since no damage was noted throughout this loading spectrum. The slope of the stress–strain curve showed perfect linearity and no damage development was observed visually by backlight illumination. This methodology was confirmed by inspecting the edge of the specimen using optical microscopy.

In our study, two types of static tensile tests were performed, namely static tests to failure and interrupted tests in which the specimens were loaded to a specific load level for three repetitions. The chosen load levels were 5, 7.5, 10, 12.5, 15 and 17.5 kN. In the case of the interrupted tests, the crack density was determined via visual inspection (aided via back light illumination) in the central 50 mm of the specimens.

2.2.2. Fatigue testing. Fatigue tests were performed in accordance with ASTM D3479 [43]—frequency 4 Hz, $R = 0.1$. The testing load ranges employed in this study were between 5 and 7.5 kN, which corresponds to 114 and 170 MPa, respectively. Fatigue tests were performed for a

maximum of 10^5 cycles and interrupted every 10^4 cycles in order to determine the crack density in the central region of the specimen.

In addition, the stiffness decay as a function of cycles was monitored using the displacement data from the test machine during the fatigue tests. This was used to give an indication of the damage state within the sample.

2.2.3. Healing protocol. Two different healing agents were used for repair, Resintech RT151 and an in-house toughened epoxy blend (further referred to as THA). The constituents of this blend are 50 wt% of Epon828 (Polysciences, Inc. Europe), 30 wt% of poly(propylene glycol) diglycidyl ether ($M_n = 380$) (Sigma-Aldrich) and, 20 wt% of Hypox RA840 (Emerald). The first constituent of THA is Bisphenol A diglycidyl ether (DGEBA) and the second a reactive diluent used to reduce the viscosity. Hypox RA840 is a DGEBA based resin system with a carboxyl-terminated butadiene acetonitrile (CTBN) adduct on 19% of epoxy monomers. This CTBN adduct precipitates to approximately 50 μm rubber particles during cure in order to increase the fracture toughness [44]. Further information on this healing agent is provided in [45].

During the study, in contrast to [46–48], no sensor system was used to determine damage initiation in the specimen, as it was out of the scope of this research study. However, the vascule could be used as a pressure drop sensor by adapting the commercial available comparative vacuum monitoring (CVM™) SHM technique, which upon detection of a damage event, would trigger resin mixing and delivery into the vascule. It was decided to load the specimen to a specific state under static or fatigue loading in order to initiate damage in the specimens. Specimens were tested to either a static load of 15 kN (350 MPa) or fatigue loaded for 50 000 cycles at a load range of 0.6–6 kN (maximum stress of 140 MPa).

Prior to healing, the sides of the specimen were sealed leaving the access to the two sides of the vascules open with one-sided adhesive release tape in order to simulate a larger continuous component.

For infusion, the vascule was first flushed through with the healing resin in order to remove entrained air (within the delivery system and vascule). At this stage, the resin remains within the vascule, and due to the limited pressure difference is unable to infuse further into the adjoining matrix cracks. To ensure the infusion of these matrix cracks, a closed-system is required such that the internal pressure reaches a threshold value to force healing resin into the matrix cracks (this threshold value is dependent upon the crack width relative to the vascule area). The formation of a closed system was readily attained by sealing one side of the vascularized specimen whilst maintaining open access on the opposite side for delivery of the resin.

Resin infusion was performed using a syringe pump (Nexus 6000, Chemyx Inc.) at a flow rate of 0.2 ml min^{-1} for 10 min Specimens were then cured for 1 h at 65 °C for the RT151 resin system, and for 1 h at 45 °C (ramp up rate 2 °C min^{-1} for both resin systems) and three days at ambient temperature for the THA resin system.

Post healing, the specimens were reloaded to 15 kN (350 MPa) or exposed to 50 000 cycles for static and fatigue healing tests, respectively.

The healing performance for the static tests is defined as follows:

$$\eta_{\text{static},E} = \frac{E_{\text{healed}} - E_{\text{damaged}}}{E_{\text{pristine}} - E_{\text{damaged}}},$$

where E_{pristine} is the stiffness during the first loading cycle, E_{damaged} is the stiffness during the first unloading cycle and E_{healed} the stiffness during the loading cycle after the healing event.

In addition, the efficiency in terms of the loss of linear behaviour during the static testing is defined as follows:

$$\eta_{\text{static,LL}} = \frac{\sigma_{\text{LL}_{\text{healed}}}}{\sigma_{\text{LL}_{\text{pristine}}}}$$

$\sigma_{\text{LL}_{\text{pristine}}}$ and $\sigma_{\text{LL}_{\text{healed}}}$ correspond to the stress when the stress–strain behaviour deviates by 10 MPa from the initial linear behaviour for the pristine and healed specimen, respectively.

The healing performance for the fatigue tests is defined as follows;

$$\eta_{\text{fatigue}} = \frac{N_2 - N_1}{N_1},$$

where N_1 is the number of cycles after which healing occurred (50 000 cycles in this case) and N_2 the total number of cycles after which the specimen had the same stiffness as prior to the healing event.

3. Results and discussion

3.1. Influence on static properties

Figure 2(i) illustrates a typical stress–strain plot for the reference and vascularized specimens. Similar failure sequences were observed for both types of specimen (refer to figures 2(ii) and (iii)): for loads below 200 MPa, no damage is present in the specimens as observed by backlight illumination. At this load threshold, the first transverse damage is initiated. Incremental increases in load, resulted in an higher transverse crack density and a reduction in stiffness. This stiffness decay stabilizes at around 250 MPa. Ply splitting due to the biaxial tensile stress state in the 0° layer, is observed for both configurations at similar load levels and occurs nearly immediately prior to final failure. Fibre failure is observed in the failed specimens along the gauge length and in the end tab region.

There was no significant difference between the two configurations in terms of strength and stiffness. The reference specimen failed at 471 ± 31 MPa (one standard deviation) and the vascularized at 462 ± 21 MPa. The stiffness for the reference and vascularized specimen was 25.4 ± 1.3 GPa and 24.5 ± 1.3 GPa, respectively. The slight decrease in strength (2%) and stiffness (4%) observed for vascularized

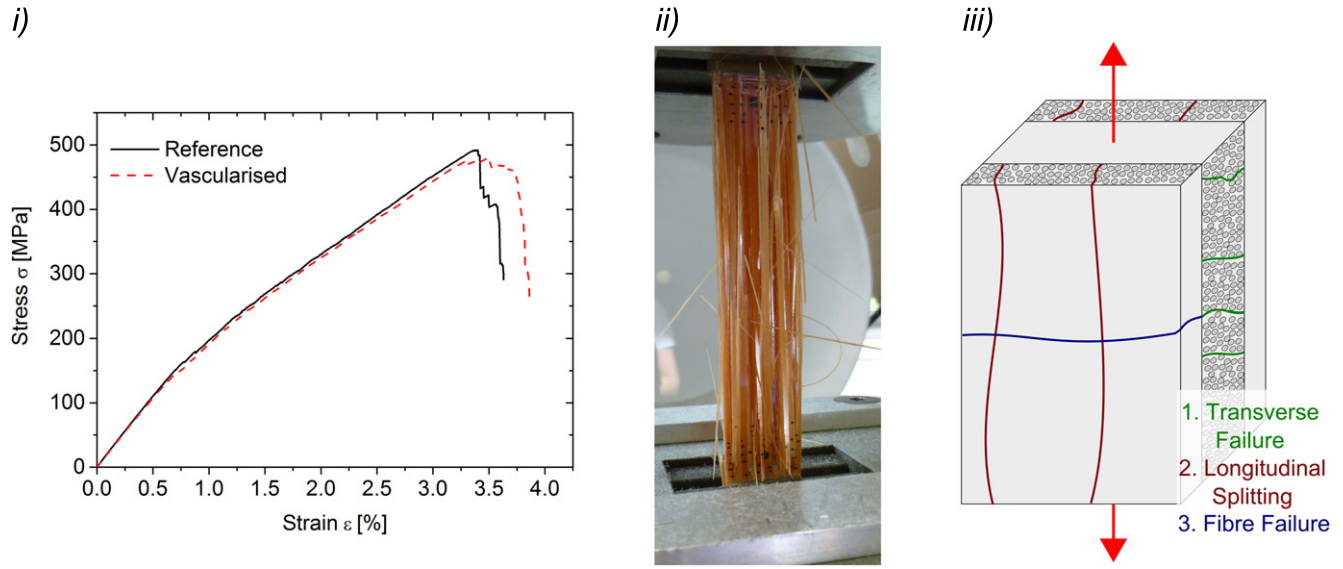

Figure 2. (i) Typical tensile test results , (ii) failed specimen and (iii) schematic of the failure sequence.

specimens is within the experimental scatter. This result is expected as the volume removed by the vascule is negligible (approximate 0.5%) and it is in accordance with the observations made by Kousarkis *et al* [25].

A key objective of the interrupted tests was to capture and understand the influence of the vascule upon damage formation. Figure 3(i) shows the transverse crack density as a function of applied maximum strain, figure 3(ii) the stiffness decay as a function of applied strain and figure 3(iii) the stiffness decay as a function of crack density. These results indicate that until reaching a strain level of approximately 0.7%, no transverse cracking was observed in either specimen configuration. As the applied strain increases further, the transverse crack density also steadily increases towards specimen failure. This is also shown in figure 3(iv) where the increment of crack density with applied strain is shown by backlight illumination photography. An inverse trend is observed in the stiffness decay as a function of the applied strain. Until reaching a maximum strain level of approximately 1%, the effect of transverse cracking seems to be negligible on the stiffness decay. This corresponds to a crack density of approximately 0.11 cracks mm^{-1}. As expected, for higher strain values, as the crack density increases, the stiffness also decreases.

Similarly to the 'static tests to failure' tests, no significant influence of the vasculature upon the damage progression can be observed. Therefore, for static applications it can be stated that the introduction of one vascule with 20 mm spacing has no measurable knockdown on the static mechanical performance.

3.2. Influence on fatigue properties

The results for the stiffness decay and crack density, as a function of fatigue cycles, tested for both configurations is shown in figure 4. Similar to the static testing, no significant influence on the damage formation and stiffness decay was observed due to the introduction of the vasculature. For the lowest load intensity of 5 kN (114 MPa), the reduction in stiffness is 3%, whereas for the fatigue tests with a maximum loading of 7.5 kN (170 MPa) a reduction of 15% was observed. It was noted that the damage formed during the first 50 000 cycles, after which the stiffness reduction stabilizes (see figure 4(i)).

No difference in the damage pattern in the 90_8° layers was observed for reference and vascularized specimens. No ply splitting was also observed in the 0_4° layers for the reference specimen, however, localized ply splitting occurred at the 0_4° plies where the transverse damage was located. This localized damage is due to the local stress transfer from the 90_8° to the 0_4° layer. Due to the localized reduction of the cross-section of the 0_4°, this stress concentration is increased leading to localized splitting.

3.3. Healing results

3.3.1. Static tests. Typical stress–strain curves are shown in figure 5 for the two healing agent systems, for before and after healing.

By infusing healing agents via vascules it is possible to completely recover the stiffness with both healing resin systems. The stiffness recovery $\eta_{\text{static},E}$ is 145 ± 23% and 114 ± 38% for the RT151 and THA healing resin, respectively. The stiffness decay of the specimens is due to the transverse damage in the 90_8° layer, which leads to a localized stress transfer to the 0_4° due to the material discontinuity in the 90_8° layer. This discontinuity leads to a reduction of the effective transverse modulus of the 90_8° layer [41]. Therefore the mechanical properties of the healing resin in terms of stiffness and strength are secondary, as long as there is sufficient stress transfer between the healing agent and the host matrix.

In contrast, the healed specimens deviated from the initial linear part at around 160 MPa and 140 MPa for RT151 and

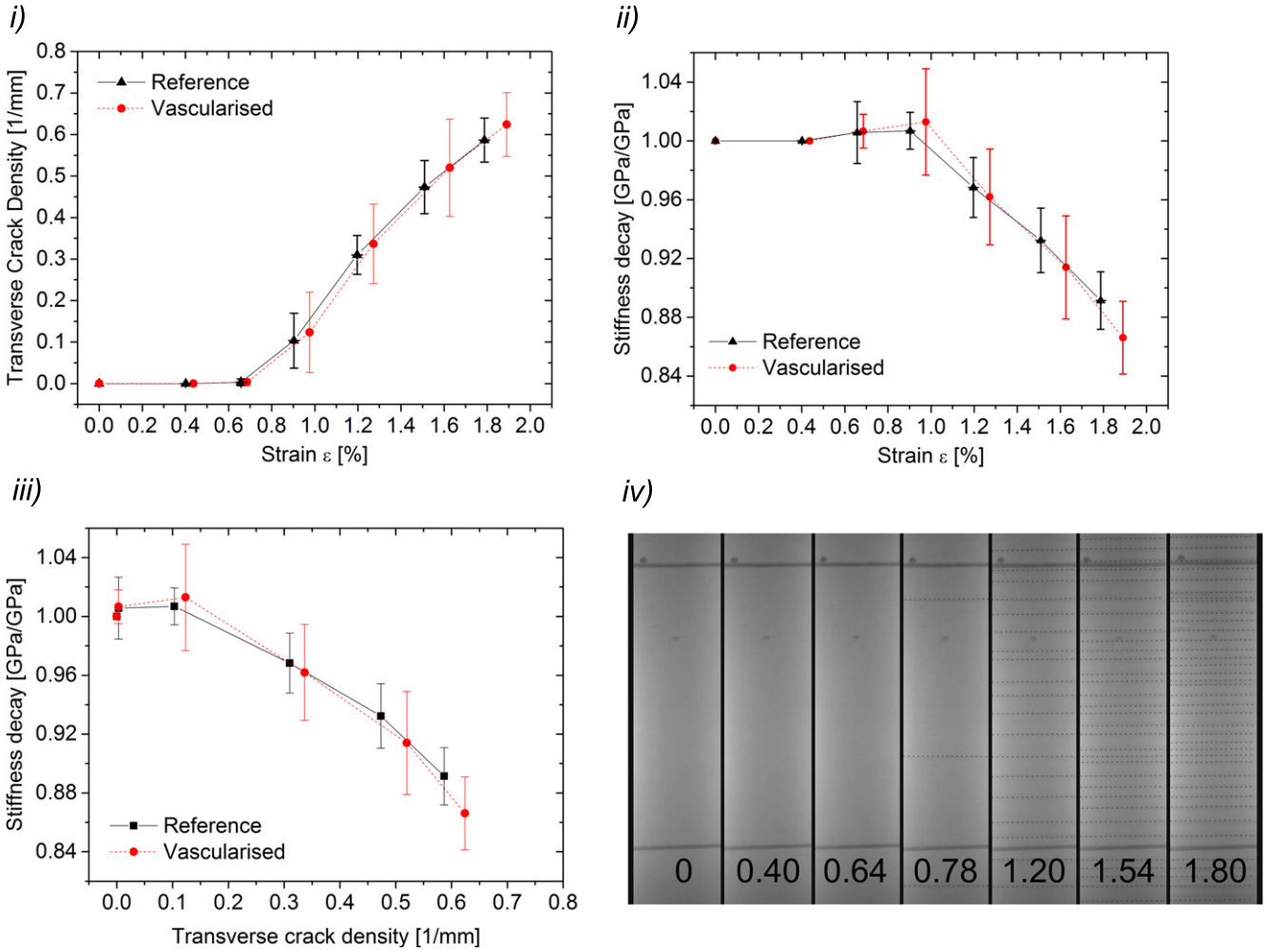

Figure 3. (i) Transverse crack density as a function of strain, (ii) stiffness decay as a function of strain for specimens with and without vascules, (iii) stiffness decay as function of transverse crack density and (iv) backlight images of the development of the damage pattern (highlighted) for a reference specimen (maximum applied strain level noted in percent). Error bars correspond to one standard deviation.

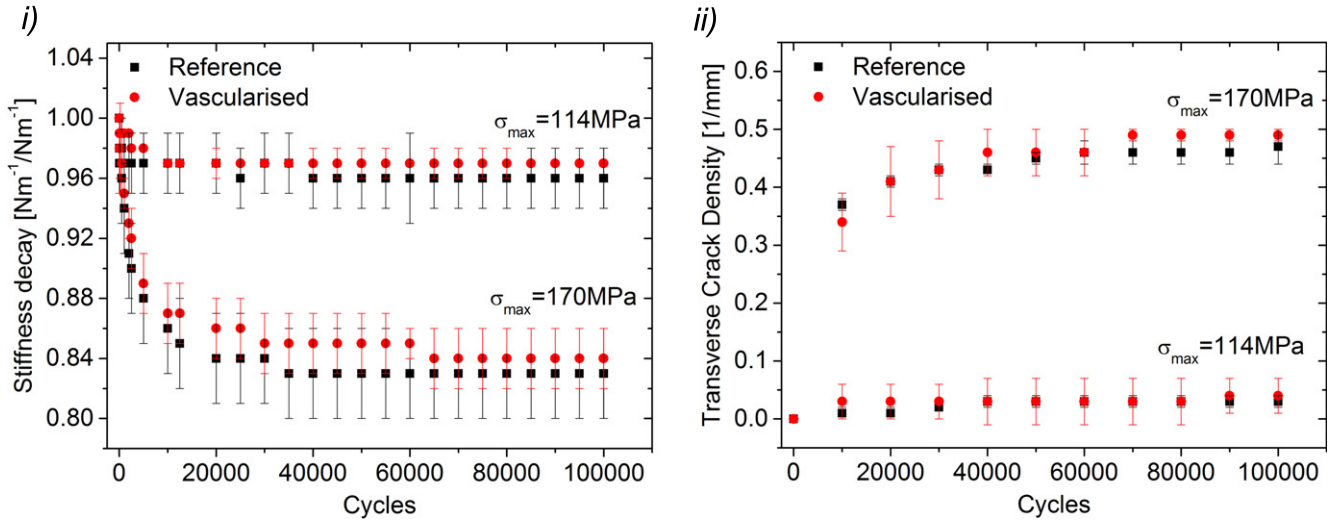

Figure 4. (i) Stiffness decay and (ii) crack density as a function of cycles. Error bars correspond to one standard deviation.

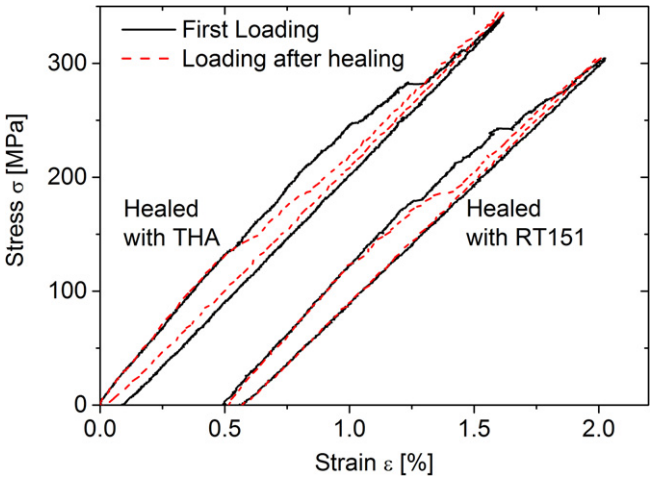

Figure 5. Typical stress–strain curves for before and after healing for the specimens healed with THA and RT151 resin systems. Note: specimen healed with RT151 is offset for visibility.

THA healing systems, respectively. This value is lower than that achieved by one of the pristine configurations where damage began to develop at 220 MPa. This leads to healing efficiency values $\eta_{\text{static,LL}}$ of $74 \pm 14\%$ and $67 \pm 11\%$ in terms of the load carrying capability for RT151 and THA, respectively. It has been observed during the experiments (via backlight illumination) that macroscopically, the damage reopens after healing at locations where the damage developed at the first loading cycle. This reopening process occurs at all locations in a relatively short time interval, whereas during initial testing a progressive damage development was observed (refer to figure 3). The reopening of the damage is dependent on the failure of the resin rich zone created during the healing process. Ideally, the healing resin should match the mechanical properties of the host matrix and provide good adhesion. However, using the host matrix material as healing agent was not a viable option as a ambient temperature infusion was envisaged. At ambient temperature, the 913 epoxy resin system is a thixotropic fluid making it impractical for infusion. An increase in temperature for the infusion was not considered as it would increase the process complexity and also reduce the working time of the resin. In addition, low temperature healing agents are preferable for an in-service application, as heating locally could lead to local distortions in the structure.

One key limitation of an extrinsic healing agent is the need for low viscosity due to the limited width of the damage plane. Figure 6 shows a micrograph of the edge of the specimen and SEM images of the transverse damage within the 90_8° layer. Similar damage was observed for both the static and fatigue loading. The damage meanders through the matrix along the glass fibres creating a material fault. The crack has an approximate width of 8 μm along the thickness of the 90_8° layer and the width of the specimen. During static and fatigue testing, the damage propagates instantaneously in a macroscopic way. However, the accepted damage mechanism is that local stress concentrations first lead to fibre–matrix debonding and microscopic matrix, which then coalesce to create macroscopic transverse damage [29, 30]. In a next step, delaminations are introduced at the tip of the transverse damage [40].

For all infusion tests, success was visually noted as the translucent transverse damage became opaque during the resin ingress of the damage site, when ascertained via through-thickness illumination. In addition, resin leaking out of the transverse damage at the edges of the specimen was visible. However, it is not possible to ascertain that the entire damage volume is wetted out by the healing agent as some parts may lack connectivity to the vascular network, some air may be entrained during the injection process or closed end cracks of the meandering transverse damage pattern may not be infused. The presence of these defects acts as stress concentrators, leading to reopening of the healed transverse damage.

Resintech RT151 is a low viscosity epoxy resin (typically 0.1 Pa s as stated by the manufacturer) and has a lower viscosity than THA (typically 0.75 Pa s). The infusion of the damage site with the more viscous resin is limited, leading to lower healing efficiency values and higher standard deviations. However, it is expected that the toughened nature of the resin will have beneficial results for progressive damage formations, such as delamination growth or fatigue damage.

3.3.2. Fatigue tests. Figure 7 shows the stiffness recovery as a function of cycles under a fatigue loading of 6 kN (140 MPa).

It should be noted, that the applied load intensity of 140 MPa is in the loading range where the loss of load linearity occurs for the healed specimen. During static loading, the damage reopened at a stress of 140–160 MPa for the THA and RT151 healing agents. Therefore, during preliminary fatigue tests at higher stress levels, the damage developed during the first cycles (refer to figure 5). Lower load level fatigue tests were not observed to introduce sufficient damage into the undamaged structure (refer to figure 4) and, therefore, the healing resin can be isolated and assessed as the limiting factor in the stiffness recovery in this experiment.

During the first 50 000 cycles, the stiffness decays by 7% and stabilizes at this level for the next 50 000 cycles. After healing, the stiffness is recovered fully for both healing resins and then drops within 2500 cycles by 5%. This rapid stiffness decay is due to damage reopening during the initial cycles. This behaviour is thought to be attributed to incomplete infusion acting as a stress concentrator, insufficient adhesion between the healing agents or inadequate mechanical properties of the healing agent. Further studies in developing suitable physical and mechanical properties of healing agents are required to address all these phenomena. Furthermore, it may well be the case that discrete matrix damage is present in the matrix that does not have vascule connectivity and hence is unable to be infused. As a result, new damage might be developing during the first re-loading cycles, similar to the case of the static healing event.

For the toughened resin system the stiffness decay is slowed leading to an additional 30 000 cycles before reaching

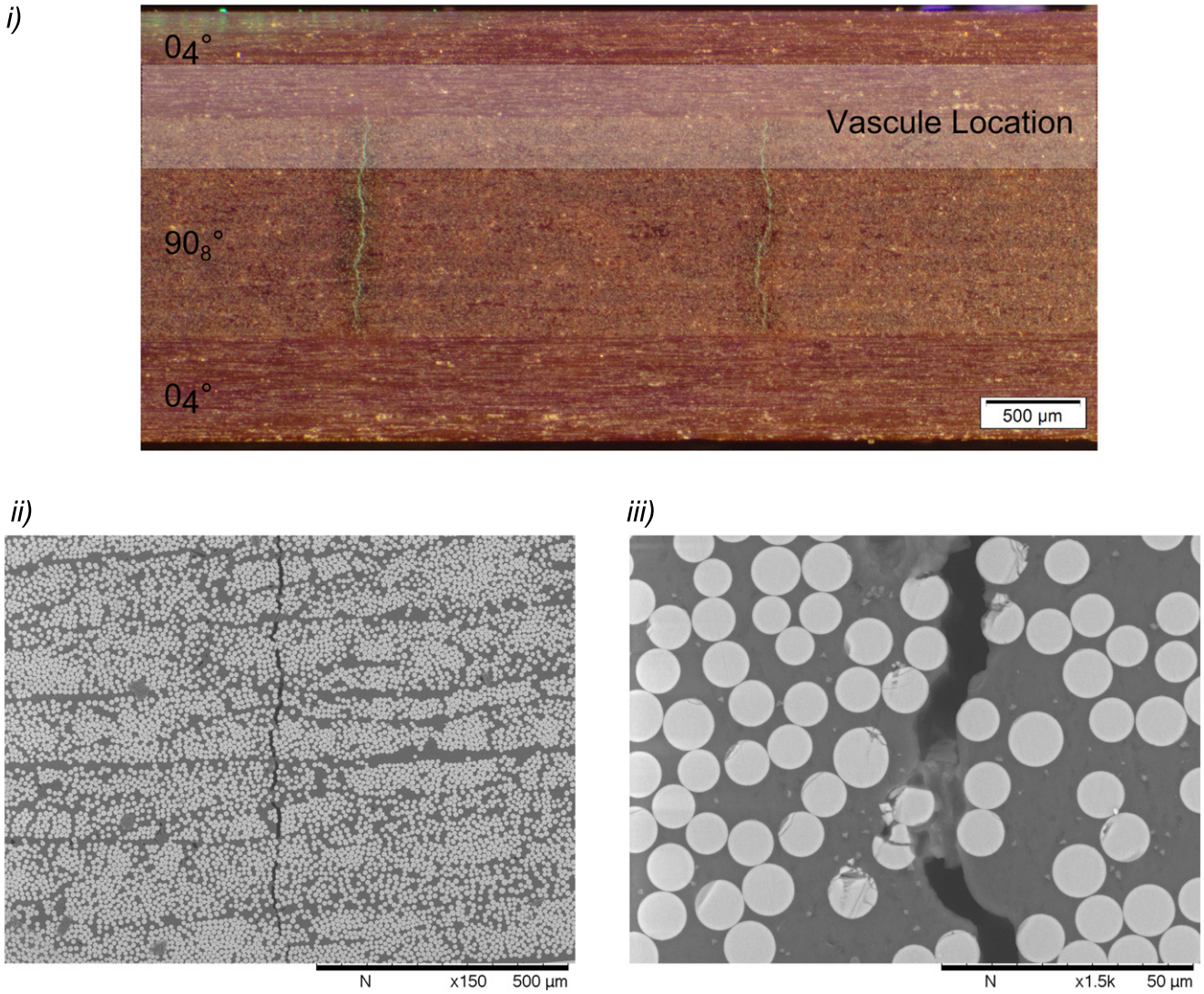

Figure 6. (i) Optical micrograph of the edge of the specimen. Damage highlighted with UV dye penetrant, the location of a vascule is indicated, (ii) and (iii) SEM micrographs showing the transverse damage in the 90_8° layer.

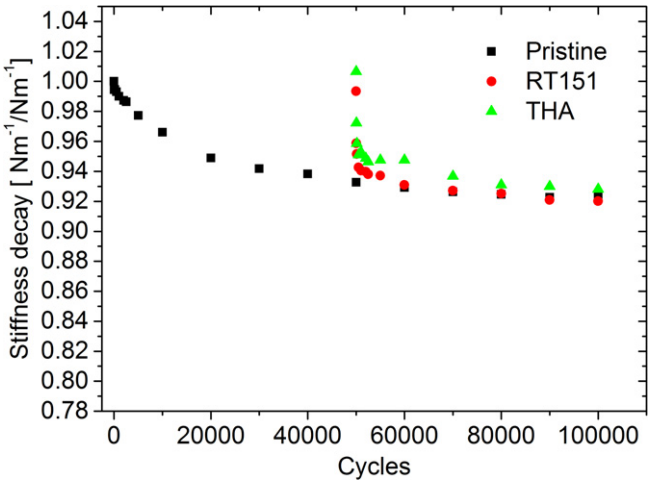

Figure 7. Stiffness decay as a function of cycles (mean values of three specimens). Fatigue loading at 140 MPa.

the reduced stiffness as observed prior to the healing process, leading to a healing efficiency of 60%. The RT151, however, loses its healing capability within 10 000 cycles, resulting in an efficiency of just 20%.

4. Conclusion and future work

In this work, the effect of the introduction of a linear vascular network into a cross-ply laminate on the static and fatigue tensile properties has been studied. The vascule was placed on the 0/90 interface in order to be able to address not only the transverse damage, but also delaminations that might propagate along this interface. It can be concluded that the embedment of such a sparse vasculature into the 0/90 interface does not have detrimental effects on mechanical

performance under tensile static and fatigue loading as similar mechanical properties and failure mechanisms are observed.

In addition, a commercial low viscosity epoxy resin (RT151, Resintech) and a toughened epoxy system were successfully used to fully recover stiffness under static conditions. Under fatigue conditions these same healing agents proved to be unsuitable due to their poor mechanical performance. However, future optimized healing agents could lead to better long term recovery of transverse damage.

One possible approach for these optimized healing agents would be a two step approach similar to conventional metal or FRP bonding, where the surface is first activated by increasing the roughness, then cleaned and degreased and then the two parts bonded together. The first chemical agent could be delivered to the damage plane in order to functionalize the fracture surface and remove any debris present in the fracture plane, then in a second step would see delivery of the healing agent.

The miniaturization and optimization of the manufacturing process for vascules also needs further development. Currently, the vascule is generated by the introduction of a preform which is subsequently removed by mechanical, chemical or thermal, means leading to both laborious and time consuming processes which is not scalable to large structural applications. Also, the need to remove the preform limits the diameter to $>200\,\mu$m (for practical purposes), which corresponds to 2 ply thicknesses leading to the need to cut fibres in order to prevent the generation of excessive resin pockets. As shown during this study, the effect of cutting fibres is negligible when the vascule is oriented in the loading direction. However, when vascules are loaded off-axis, a reduction in strength is expected. One possible solution is the incorporation of vascules composed of a porous wall in order to eliminate the need to remove the preform after the curing process. This is the subject of a separate ongoing study.

A final step for improvement is the development of a feedback system which indicates that not only the healing process has taken place, but that it has been completed successfully.

Even though many challenges remain in deploying self-healing in structural in-service applications, the work to date has shown the ability to recover from damage events by the introduction of a healing agent through a vascular network. If coupled with a complementary SHM solution, these technologies will lead the way to smart structures that can autonomously sense and recover following a damage event.

Acknowledgments

The authors would like to thank the UK Engineering and Physical Sciences Research Council (EPSRC) (EP/G036772), Fundació Obra Social la Caixa and the European FP7 HIPOCRATES (ACP3-GA-2013-605412) for funding this project. We would also like to thank Daniel T Everitt for his support on developing the healing agents, Ian Gent for his help with the SEM and Ian Chorley and Glenn Wallington for their assistance in the laboratory, and Martin F Cicognani from Hubron Speciality for his support and for providing the HyPox RA840.

References

[1] Blaiszik B J, Kramer S L B, Olugebefola S C, Moore J S, Sottos N R and White S R 2010 Self-healing polymers and composites *Annu. Rev. Mater. Res.* **40** 179–211

[2] Van der Zwaag S, Grande A M, Post W, Garcia S J and Bor T C 2014 Review of current strategies to induce self-healing behaviour in fibre reinforced polymer based composites *Mater. Sci. Technol.* **30** 1633–41

[3] Kessler M R 2007 Self-healing: a new paradigm in materials design *Proc. Inst. Mech. Eng.* G **221** 479–95

[4] Wu D Y, Meure S and Solomon D 2008 Self-healing polymeric materials: a review of recent developments *Prog. Polym. Sci.* **33** 479–522

[5] Norris C J, Bond I P and Trask R S 2013 Healing of low-velocity impact damage in vascularised composites *Composites* A **44** 78–85

[6] Zhong N and Post W 2015 Self-repair of structural and functional composites with intrinsically self-healing polymer matrices: a review *Composites* A **69** 226–39

[7] Yang T, Zhang J, Mouritz A P and Wang C H 2013 Healing of carbon fibre–epoxy composite T-joints using mendable polymer fibre stitching *Composites* B **45** 1499–507

[8] White S R, Sottos N R, Geubelle P H, Moore J S, Kessler M R, Sriram S R, Brown E N and Viswanathan S 2001 Autonomic healing of polymer composites *Nature* **409** 794–7

[9] Bleay S, Loader C, Hawyes V, Humberstone L and Curtis P 2001 A smart repair system for polymer matrix composites *Composites* A **32** 1767–76

[10] Pang J W C and Bond I P 2005 A hollow fibre reinforced polymer composite encompassing self-healing and enhanced damage visibility *Compos. Sci. Technol.* **65** 1791–9

[11] Trask R S and Bond I P 2006 Biomimetic self-healing of advanced composite structures using hollow glass fibres *Smart Mater. Struct.* **15** 704–10

[12] Coope T S, Wass D F, Trask R S and Bond I P 2014 Repeated self-healing of microvascular carbon fibre reinforced polymer composites *Smart Mater. Struct.* **23** 115002

[13] Coope T S, Wass D F, Trask R S and Bond I P 2013 Metal triflates as catalytic curing agents in self-healing fibre reinforced polymer composite materials *Macromol. Mater. Eng.* **299** 208–18

[14] Jin H, Mangun C L, Stradley D S, Moore J S, Sottos N R and White S R 2012 Self-healing thermoset using encapsulated epoxy-amine healing chemistry *Polymer* (*Guildf*) **53** 581–7

[15] Trask R S and Bond I P 2010 Bioinspired engineering study of Plantae vascules for self-healing composite structures *J. R. Soc. Interface* **7** 921–31

[16] Kozola B D, Shipton L A, Natrajan V K, Christensen K T and White S R 2010 Characterization of active cooling and flow distribution in microvascular polymers *J. Intell. Mater. Syst. Struct.* **21** 1147–56

[17] Stehmeier H and Speckmann H 2004 Comparative vacuum monitoring (CVM) monitoring of fatigue cracking in aircraft structures *2nd European Workshop on Structural Health Monitoring* (*Munich*)

[18] Norris C J, Bond I P and Trask R S 2011 The role of embedded bioinspired vasculature on damage formation in self-healing carbon fibre reinforced composites *Composites* A **42** 639–48

[19] Norris C J, Bond I P and Trask R S 2011 Interactions between propagating cracks and bioinspired self-healing vascules embedded in glass fibre reinforced composites *Compos. Sci. Technol.* **71** 847–53

[20] Toohey K S, Sottos N R, Lewis J A, Moore J S and White S R 2007 Self-healing materials with microvascular networks *Nat. Mater.* **6** 581–5
[21] Williams H R, Trask R S, Knights A C, Williams E R and Bond I P 2008 Biomimetic reliability strategies for self-healing vascular networks in engineering materials *J. R. Soc. Interface* **5** 735–47
[22] Wu A S, Coppola A M, Sinnott M J, Chou T-W, Thostenson E T, Byun J-H and Kim B-S 2012 Sensing of damage and healing in three-dimensional braided composites with vascular channels *Compos. Sci. Technol.* **72** 1618–26
[23] Hamilton A R, Sottos N R and White S R 2010 Local strain concentrations in a microvascular network *Proc. Soc. Exp. Mech. Inc.* **67** 255–63
[24] Kousourakis A and Mouritz A P 2010 The effect of self-healing hollow fibres on the mechanical properties of polymer composites *Smart Mater. Struct.* **19** 085021
[25] Kousourakis A, Bannister M K and Mouritz A P 2008 Tensile and compressive properties of polymer laminates containing internal sensor cavities *Composites* A **39** 1394–403
[26] Kousourakis A, Mouritz A P and Bannister M K 2006 Interlaminar properties of polymer laminates containing internal sensor cavities *Compos. Struct.* **75** 610–8
[27] Huang C-Y, Trask R S and Bond I P 2010 Characterization and analysis of carbon fibre-reinforced polymer composite laminates with embedded circular vasculature *J. R. Soc. Interface* **7** 1229–41
[28] Coppola A M, Thakre P R, Sottos N R and White S R 2014 Tensile properties and damage evolution in vascular 3D woven glass/epoxy composites *Composites* A **59** 9–17
[29] Lubineau G and Rahaman A 2012 A review of strategies for improving the degradation properties of laminated continuous-fiber/epoxy composites with carbon-based nanoreinforcements *Carbon* (*NY*) **50** 2377–95
[30] Gamstedt E and Sjögren B 1999 Micromechanisms in tension-compression fatigue of composite laminates containing transverse plies *Compos. Sci. Technol.* **59** 167–78
[31] Jalalvand M, Wisnom M R, Hosseini-Toudeshky H and Mohammadi B 2014 Experimental and numerical study of oblique transverse cracking in cross-ply laminates under tension *Composites* A **67** 140–8
[32] Greenhalgh E, Singh S and Nilsson K-F 2000 Mechanisms and modelling of delamination growth and failure of carbon-fibre reinforced skin-stringer panels *Composite Structures: Theory and Practice STP 1383* ed P Grant and C Q Rousseau (West Conshohocken, PA: American Society for Testing and Materials) pp 49–71
[33] Hull D 1994 Matrix-dominated properties of polymer matrix composite materials *Mater. Sci. Eng.* A **184** 173–83
[34] Manfredi E, Cohades A, Richard I and Michaud V Assessment of solvent capsule-based healing for woven E-glass fibre-reinforced polymers *Smart Mater. Struct.* **24** 15019
[35] Patrick J F, Hart K R, Krull B P, Diesendruck C E, Moore J S, White S R and Sottos N R 2014 Continuous self-healing life cycle in vascularized structural composites *Adv. Mater.* **26** 4302–8
[36] Jones A R, Blaiszik B J, White S R and Sottos N R 2013 Full recovery of fiber/matrix interfacial bond strength using a microencapsulated solvent-based healing system *Compos. Sci. Technol.* **79** 1–7
[37] Nielsen C and Nemat-Nasser S 2015 Crack healing in cross-ply composites observed by dynamic mechanical analysis *J. Mech. Phys. Solids* **76** 193–207
[38] Zako M and Takano N 1999 Intelligent material systems using epoxy particles to repair microcracks and delamination damage in GFRP *J. Intell. Mater. Syst. Struct.* **10** 836–41
[39] Singh S and Greenhalgh E S 1998 Micromechanics of interlaminar fracture in carbon fibre reinforced plastics at multidirectional ply interfaces under static and cyclic loading *Plast. Rubber Compos. Process. Appl.* **27** 220–6
[40] Takeda N and Ogihara S 1994 Initiation and growth of delamination from the tips of transverse cracks in CFRP cross-ply laminates *Compos. Sci. Technol.* **52** 309–18
[41] Talreja R 1985 Transverse cracking and stiffness reduction in composite laminates *J. Compos. Mater.* **19** 355–75
[42] ASTM International 2014 *ASTM D3039-14 Standard Test Method for Tensile Properties of Polymer Matrix Composite Materials* (West Conshohocker, PA: ASTM International) pp 1–13
[43] ASTM International 2007 *ASTM D3479/D3479M-96* (*Reapproved 2007*) *Standard Test Method for Tension–Tension Fatigue of Polymer Matrix Composite* (West Conshohocker, PA: ASTM International) pp 1–6
[44] Yee A F and Pearson R A 1986 Toughening mechanisms in elastomer-modified epoxies part 1 mechanical studies *J. Mater. Sci.* **21** 2462–74
[45] Everitt D T, Luterbacher R, Coope T S, Trask R S, Wass D F and Bond I P 2015 Optimisation of epoxy blends for use in extrinsic self-healing fibre-reinforced composites *Polymer* **69** 283–92
[46] Minakuchi S, Sun D and Takeda N 2014 Hierarchical system for autonomous sensing-healing of delamination in large-scale composite structures *Smart Mater. Struct.* **23** 115014
[47] Norris C J, White J A P, McCombe G, Chatterjee P, Bond I P and Trask R S 2012 Autonomous stimulus triggered self-healing in smart structural composites *Smart Mater. Struct.* **21** 1–10
[48] Trask R S, Norris C J and Bond I P 2014 Stimuli-triggered self-healing functionality in advanced fibre-reinforced composites *J. Intell. Mater. Syst. Struct.* **25** 87–97